



Contents lists available at ScienceDirect

Aerospace Science and Technology

www.elsevier.com/locate/aescte



Spark ignition and stability limits of spray kerosene flames under subatmospheric pressure conditions

Yakun Huang^{a,b}, Xiaomin He^{a,*}, Huangwei Zhang^{b,*}, Jieli Wei^{a,c}, Daniel W.M. Sng^b

^a College of Energy and Power Engineering, Nanjing University of Aeronautics and Astronautics, Nanjing 210016, Jiangsu, China

^b Department of Mechanical Engineering, National University of Singapore, Singapore 117576, Singapore

^c Institute for Aero Engine, Tsinghua University, Beijing 100084, China

ARTICLE INFO

Article history:

Received 25 January 2021

Received in revised form 7 April 2021

Accepted 8 April 2021

Available online xxxx

Communicated by Kostas Kontis

Keywords:

Flameholder

Flame stability

Low pressure

Ignition delay

Lean blowout

ABSTRACT

Flame stability limits and ignition delay time of the flameholder are experimentally studied in this work at the pressure of 0.03 – 0.06 MPa, Mach number of 0.1 – 0.3, and temperature of 320 K – 800 K. The results indicate that the reduction in equivalence ratios of lean ignition and blowout can be achieved by the increase in pressure or Mach number. Temperature rise will first increase and then decrease the lean ignition equivalence ratio. While increasing lean blowout equivalence ratio was observed with increasing temperature. The envelope of the stable combustion between the pressure and Mach number is measured, and the lowest temperature of successful ignition is 300 K, acquired at Mach 0.1 and 0.06 MPa. Besides, the correlation between the equivalence ratios of flame stability and inlet parameters, such as pressure, Mach number, temperature, is developed. The ignition process of the flameholder is imaged, and the ignition delay time decreases with increased pressure or temperature. The ignition delay time is shown first to decrease and then increase with the increase in Mach number.

© 2021 Elsevier Masson SAS. All rights reserved.

1. Introduction

The propulsion system has been developing in the direction of the higher altitude and speed, which promotes the progress of air-breathing hypersonic vehicles, such as ramjet [1], scramjet [2], and combined cycle engines [3,4]. However, for any propulsion system that uses liquid fuel, increasing the flight altitude poses significant challenges to flame stability [5], especially extinction and reignition at high-altitude [6], such as 10 – 40 km, combining with the low pressure and temperature.

With the inlet pressure decrease, the flame stability deteriorates and combustion efficiency decreases; even oscillatory combustion and global flame extinction may occur [7]. Previous studies have confirmed that the combustion efficiency deteriorates sharply from 75% with the localized quenching when the pressure is smaller than 0.07 MPa, and the combustion cannot proceed at 0.03 MPa [8]. Hence, it is imperative to address this scientific problem associated with flame stability in a low-pressure environment, motivated by tremendous development needs.

Previous studies on low-pressure combustion are mainly focused on the fields of aerospace [9], plateau fire prevention [10],

and batteries [11]. For instance, NASA conducts systematic research on spray combustion performance under high altitude conditions [12]. The results indicate that compared with the atmospheric conditions, the fuel atomization and distribution under low pressure are worse, which leads to a narrower flame stabilization boundary. Meanwhile, reactant mixing is weak, resulting in inadequate combustion and low energy conversion efficiency. Black [13] conducted experimental research based on a rectangular ramjet model and found that the combustion efficiencies of 28% to 39% were obtained at the flight altitude of 8.4 km (0.034 MPa). Other researchers used optical diagnostic techniques [14,15] to study the effect of pressure on the flame stability limit, ignition process, and ignition delay. Furthermore, a low-pressure ignition limit experiment was conducted by Okai [9], which demonstrated that the lowest pressure for the stable combustion of hydrogen fuel is 0.03 MPa. Meanwhile, the pressure considerably affects the flame propagation velocity, and the minimum ignition pressure increased rapidly with the increase of the velocity. Read [16] studied the high-altitude reignition of the direct-injection gas turbine combustor shown that the generated kernel's size cannot determine the ignition success, and it disintegrated rapidly when the pressure less than 0.04 MPa. Nguyen [17] found that the ignition delay time increases with decreasing pressure or temperature, which was slightly affected by the pressure when the temperature is above 700 K and changed significantly when the temperature is below

* Corresponding authors.

E-mail addresses: hxm@nuaa.edu.com (X. He), huangwei.zhang@nus.edu.sg (H. Zhang).

<https://doi.org/10.1016/j.ast.2021.106734>

1270-9638/© 2021 Elsevier Masson SAS. All rights reserved.

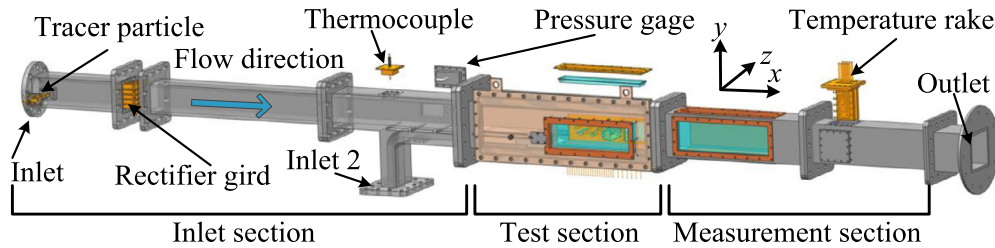


Fig. 1. Schematic of the experimental facility.

700 K. Also, the ignition delay time of RP-3 was investigated in static fluid conditions with the effect of temperature, pressure, and equivalence ratio [18]. The results confirmed again that the increase of pressure shortened the ignition time with the liquid fuel RP-3, but the velocity was not considered. Furthermore, a reduction in pressure is shown to decrease the radiative loss and chemical reaction rate, which weakens the flames. However, all of the results were obtained in premixed flame or static fluid conditions, which cannot fully mimic the practical operating conditions. To achieve reliable ignition and reignition at high altitudes, the spark ignition and flame limits must be fully understood in a low-pressure environment. However, limited studies had focused on the spray kerosene flames under high speed and subatmospheric pressure conditions. Therefore, this work aims to understand the influence of pressure on the ignition process and explore the flame stability limits under ultra-low pressure conditions.

In this paper, the flameholder installed in a rectangular channel is designed to investigate the flame stability limits and ignition delay time of kerosene spray flames under the operating conditions of pressure 0.03–0.06 MPa, Mach number 0.1–0.3 MPa, and temperature 320–800 K. The ignition process of spray kerosene flame in a combustor with flameholder is measured, and the ignition and lean blowout limits will be studied. Moreover, the envelope of stable combustion with critical pressure and Mach number is obtained at an inlet temperature of 700 K. The novelty of this paper is to explore the lower pressure flame stability limits in the high-speed flow environment, providing a reference for expanding the research on the flight envelope of the ramjet engine. The rest of this manuscript is organized as below. Section 2 will introduce the experimental system and method, and Section 3 presents the results and discussion. Our findings will be summarized in Section 4.

2. Experimental system and method

2.1. Experimental facility

The schematic of the experimental facility is shown in Fig. 1. It is comprised of three sections, i.e., inlet section, test section, and measurement section. The inlet section includes the injector of tracer particle, rectifier grid, as well as measurement point for air temperature and pressure. The second inlet (marked as “inlet 2” in Fig. 1) is designed for other research purposes and not used in the current studies. The measurement section is used for measuring exhaust gas composition and temperature.

The test section lies in the middle of the experimental facility and is a model ramjet combustor, as shown in Fig. 1. Its dimensions are 100 mm (width) \times 110 mm (height) \times 860 mm (length). Removable cover plates are mounted on the four sides of the rectangular test rig, and a quartz window with a size of 350 mm \times 110 mm fitted on one side, which allows the visual assessment of spray flame ignition and lean blowout. The inlet’s vitiated air is divided into two streams by the flameholder to form a recirculation zone. The spray flame is ignited and burns stably after the fuel is injected into the flameholder.

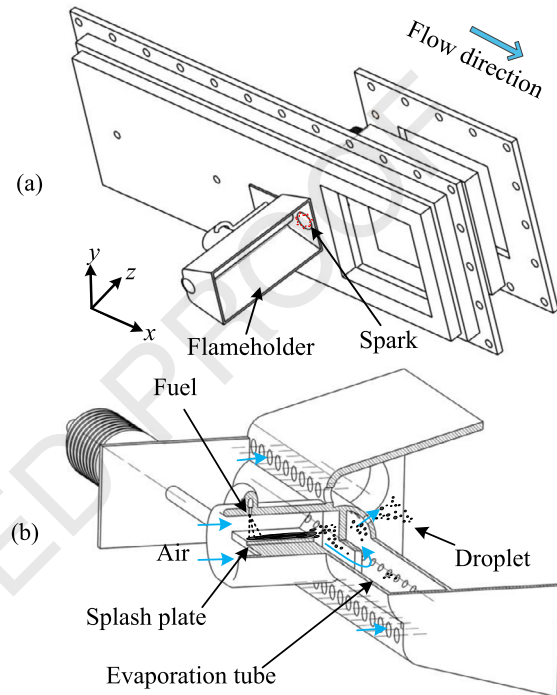


Fig. 2. Schematic of (a) the flameholder assembly and (b) flameholder.

Fig. 2(a) shows the schematic of the flameholder assembly. The flameholder is installed in the center of the test section with the blockage ratio of $\beta = 0.41$, and the plain orifice atomizer is installed at 150 mm upstream. The flameholder is optimized based on the V-gutter stabilizer, in which a round tube with 21×2 holes is installed inside the evaporation tube. The evaporation tube’s air inlet is arranged in the center of the flat top, and symmetrical holes are distributed on both sides. An orifice injector is employed in the flameholder with a diameter of 0.5 mm. The evaporation tube’s designed mass flow rates and small holes are 2.5% and 2.37% of the total flow mass rates, respectively. Fig. 2(a) demonstrated that the igniter is a surface discharge igniter plug with a diameter of 14 mm. The stored energy of the spark plug is 20 J, and its frequency is 8 Hz, in which the single duration is about 0.2 ms.

The roles of the flameholder inside the test section include: (1) liquid fuel injection and breakup, (2) fuel/oxidizer mixing, (3) ignition, as well as (4) flame stabilization with a recirculation zone. The RP-3 liquid fuel is injected vertically into the splash plate from the orifice atomizer, and the properties of the RP-3 liquid kerosene are listed in Table 1. Part of the fuel breaks up into droplets, while some impinge on the plate surface and form the liquid fuel film. Then, the liquid fuel film, moving and mixing with the air, gradually becomes thinner and breaks into droplets at the end of the splash plate [19]. When the flame stabilizes in the recirculation zone, the droplet evaporates inside of evaporation tube due to the heat transfer.

Table 1
Properties of RP-3 liquid kerosene [20,21].

Fuel	Molecular formulas	Density (kg/m ³)	Lower heating value (kJ/kg)	Viscosity (10 ⁻⁶ m ² /s)	Surface tension (N/m)	Boiling point (K)	Flash point (K)
RP-3	C ₁₂ H ₂₃	780	≥42800	≥1.25	0.023	423 – 523	311

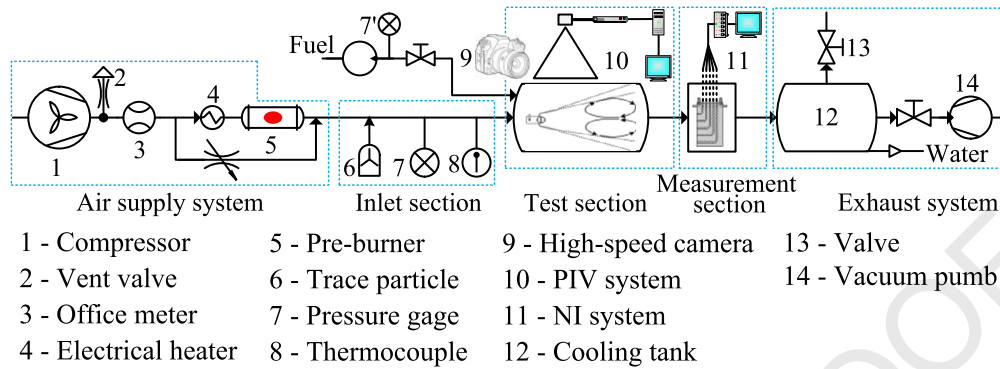


Fig. 3. Schematic of the experimental system.

2.2. Experimental method

Fig. 3 shows that the experimental system includes the air supply system, inlet section, test section, measurement section, and exhaust system. The dehumidified air with a maximum total mass flow rate of 1.5 kg/s is supplied from the compressor, and the mass flow rate is measured by an orifice plate flowmeter with an uncertainty of 0.57%. The air is heated to an inlet temperature being 320–800 K by an electric heater and a pre-burner, in which the burned gas is mixed with the fresh air to maintain the oxygen mass fraction of $20.5\% \pm 0.64\%$. The total temperature and pressure are measured by a K-type thermocouple and a pressure gauge at 350 mm and 220 mm upstream of the test section, respectively, which are also shown in Fig. 1. Both inlet temperature and pressure have an uncertainty of 0.4%. The exhaust system is composed of a cooling tank and three vacuum pumps, which can reduce the pressure to 8 kPa in the cooling tank. The fuel is supplied from the flameholder in this work, and the mass flow rates can be measured by pressure gauges with the correlations between the fuel mass flow rate \dot{m}_{fuel} and pressure drop ΔP_{fuel} , i.e.

$$\dot{m}_{fuel} = 1.8468 \Delta P_{fuel}^{0.4978} \quad (1)$$

Here the pressure drop ΔP_{fuel} is the pressure difference between the inlet and outlet of the injector, which can be measured by pressure gauges 7 and 7' (as seen from Fig. 3). Equation (1) is calibrated before and after the test by pressure gauges and an electronic scale. The uncertainties of the pressure gauges and the electronic scale are 0.4% and 0.005%, respectively.

The high-speed camera *Phantom v2012* is adopted to image the ignition process with a spatial resolution of $1,280 \times 800$ and a sampling frequency of 10,000 fps. The pixel resolution is 0.1024 – 0.1456 mm/pixel, and the time interval and exposure time are 100 μ s and 50 μ s, respectively.

In our studies, ignition and extinction are identified with image visualization criteria. The image observations are used to obtain the instantaneous fuel pressure drop when flame ignition or extinction occurs. In this method, the ignition and extinction are determined by image observation [15,22]. When the flame kernel firstly appears in the window, the ignition is considered successful, and the fuel mass flow rate is recorded at this time. If the flame is unstable and ultimately quenched, the ignition is regarded as

failed ignition. After successful ignition, the fuel mass flow rate is gradually reduced. The flame blowout occurs when the flame has completely disappeared, and the fuel mass flow rate is also recorded.

The experiment procedures of spark ignition and lean blowout of spray kerosene flames are shown in Fig. 4(a) and Fig. 4(b), respectively. In order to measure the flame stability limit, the detailed procedure is as follows: First, the fuel is supplied, and the pressure drop increases until the ignition is completed after the spark is discharged. This pressure drop ΔP_0 is marked as the initial pressure drop, at which the flame can be ignited successfully. Then, the fuel pressure drop gradually decreases with the step of ΔP to obtain the lowest pressure drop of successful ignition, and the ignition equivalence ratio can be calculated. In this experiment, the pressure gauge's degree is 0.005 MPa, namely $\Delta P = 0.005$ MPa. Besides, for lean blowout studies, a similar method is applicable through measuring the fuel pressure drop, as demonstrated in Fig. 4(b). Afterward, when carrying out the stability envelope, the lean blowout limit is obtained by adjusting the inlet conditions after ignition succeeds, such as keeping the inlet Mach number to reduce the inlet pressure or keeping the inlet pressure to increase the inlet Mach number. It is considered that the inlet condition is the flame stability envelope when the flame cannot be stabilized under the adjusted condition with various equivalence ratios.

A sequence of milestone instants is identified corresponding to various flame development stages, as shown in Fig. 5. During the ignition experiments, the fuel is first supplied at a designed flow rate, and then the high-speed camera is used to image flame morphology. Specifically, the high-speed camera is started at t_{-2} , and then the spark plug begins to discharge at t_{-1} and ends at t_0 . Note that at t_0 , the flame kernel has not appeared in all measurements reported in this paper. t_1 , t_2 , and t_3 are marked as the instants of flame kernel generation, flame growth, and stable combustion. The moments of t_1 , t_2 , and t_3 are determined by the development of the flame projected area, where the smallest flame area is achieved at t_1 . Then, after the ignition kernel is initially generated, the flame projection area increases slowly. However, the kernel projection area fluctuates after a while; it rapidly rises to the maximum value and then levels off. Hence, the start and end of the flame projection area's rapid increase are recorded as t_2 and t_3 , respectively. The detailed development will be discussed in Section 3.1.

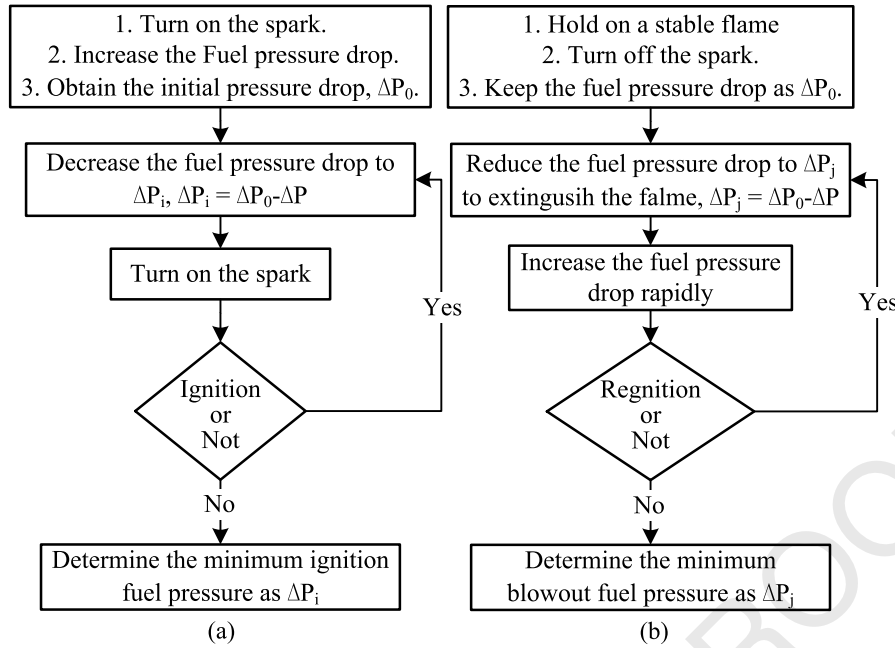


Fig. 4. Experimental procedures of (a) spark ignition and (b) blowout of spray kerosene flames.

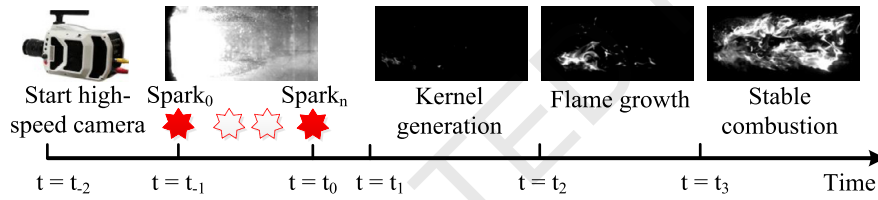


Fig. 5. Milestone instants in the flame ignition process.

Table 2
Experimental condition and uncertainty.

Variable	Method	Value	Uncertainty
Inlet temperature, T (K)	K-type thermocouple	320 – 800	0.40%
Inlet pressure, P_i (MPa)	Pressure gauge	0.03 – 0.10	0.40%
Air mass flow rate, \dot{m}_a (kg/s)	orifice plate flowmeter	0.233 – 0.775	0.57%
Inlet Mach number, Ma	$Ma = \dot{m}_a / A(\lambda RT)^{1/2}$	0.1 – 0.3	0.70%
Inlet Reynolds number, Re (10^5)	$Re = (P/RT)(\dot{m}_a/A)d/\mu$	1.377 – 4.284	0.80%
Fuel mass flow rate, \dot{m}_f 10^{-3} kg/s	$\dot{m}_f = 1.8468 \Delta P_{fuel}^{0.4978}$	0.829 – 1.784	0.40%
Equivalence ratio, φ_{total}	$\varphi_{total} = \dot{m}_f / (\dot{m}_{aqst})$	0.030 – 0.121	0.70%

2.3. Operating condition

To investigate ignition and lean blowout limits of kerosene spray flames at the reduced pressure conditions, six subatmospheric and one atmospheric pressure are studied to mimic the ramjet combustion conditions in high-altitude flights with inlet Mach number of 0.1 – 0.3 and temperature of 320 – 800 K. The influence of inlet velocity and temperature on flame stability is studied under the pressure of 0.06 MPa.

As mentioned in section 2.2, some quantities, such as inlet pressure and temperature, are directly measured in the experiments. In contrast, such as air mass flow rate and equivalence ratio are derived. The uncertainties of measured quantities are evaluated by the T-distribution assumption with the confidence factor $z = 1.96$. Besides, the probability of confidence is 95%. Then the uncertainties of the derived quantities are estimated from [23]

$$\Delta R = \left[\left(\frac{\partial R}{\partial x_1} \Delta x_1 \right)^2 + \left(\frac{\partial R}{\partial x_2} \Delta x_2 \right)^2 + \dots + \left(\frac{\partial R}{\partial x_n} \Delta x_n \right)^2 \right]^{1/2} \quad (2)$$

where R is the derived quantity, ΔR is the error limit, and Δx_i is the error limits of the measured values.

The uncertainties of measured and derived quantities are listed in Table 2. Here, m_{fuel} is the fuel mass flow rate, m_{air} is the air-flow rate, φ is the equivalence ratio, and q_{st} is the stoichiometric fuel/air ratio, which is 0.0672 for the RP-3 liquid fuel [24]. Then, one derived quantity of the air mass flow rate, as an example, can be calculated by

$$\dot{m}_{air} = 1.4089 \sqrt{\frac{(P_{air0} + \Delta P_{air})H}{T}} \quad (3)$$

where \dot{m}_a is the air mass flow rate; P_{air0} is the ambient pressure; P_{air} is the pressure upstream of the orifice plate flowmeter, both P_{air0} and P_{air} are measured by pressure gauges; H is the pressure difference between upstream and downstream of the orifice plate flowmeter, measured by U-type manometer with the uncertainty of 0.01%; T is the air temperature at orifice plate flowmeter, measured by K-type thermocouple.

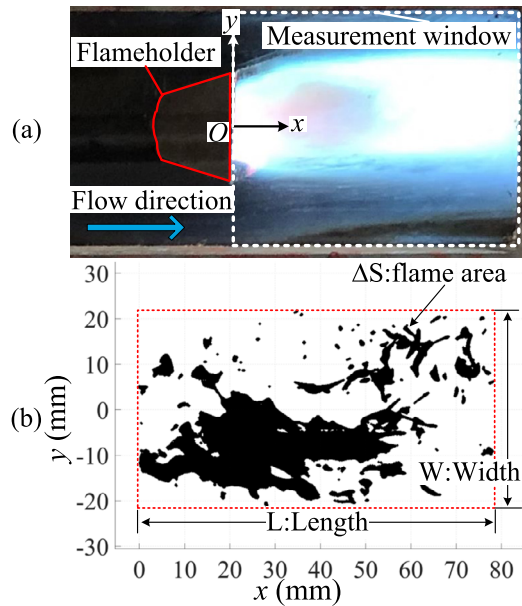


Fig. 6. Schematic of (a) the measurement window and (b) geometrical quantities of the flame.

Hence, according to Eq. (2), the uncertainty of air mass flow rate can be calculated by

$$\frac{\Delta \dot{m}_{air}}{\dot{m}_{air}} = \sqrt{\left(\frac{\Delta H}{H}\right)^2 + \left(\frac{\Delta T}{T}\right)^2 + \left(\frac{\Delta P}{P}\right)^2} = 0.57\% \quad (4)$$

2.4. Diagnostic technique

Fig. 6(a) shows the test section's measurement window, as shown in Fig. 1. The origin of the coordinate system lies at the central position of the flameholder. The flow direction is determined as the positive direction of the x -axis, as shown in Fig. 6(a). The ignition process is recorded by a high-speed camera in the white dotted box in Fig. 6(a) with a size of 120 mm \times 100 mm.

Fig. 6(b) shows the characteristic geometrical quantities extracted from optical image processing. The segmentation method of the watershed transform [25] is adopted to obtain the developing flame characteristics from the two-dimensional digital image. Then, the flame geometrical and topological quantities, including the flame projection area, length, and width, are calculated by the size of pixels covered by the flame. The flame projection area is the sum of the areas of the pixels corresponding to a flame. As shown in Fig. 6(b), the flame length L is defined as the streamwise distance between the most downstream point of the flame profile and the rear of the flameholder. The flame width W is the y -axis extent with which the binarized flame pixels can be found.

3. Results and discussion

3.1. Ignition process

The evolution of flame morphology during the spark ignition process is shown in Fig. 7. In this case, the inlet Mach number is 0.2, the temperature is 700 K, the pressure is 0.06 MPa, and the total equivalence ratio is 0.082. The flame kernel is initiated inside the flameholder and surrounds the evaporation tube after the spark plug discharges at t_0 (as shown in Fig. 5). Then at $t = 1.0$ ms, the evaporation tube temperature increases, and hence the fuel droplet evaporation is accelerated. The local vapor accumulation is conducive to initiate an ignition kernel [26,27]. The above

process is marked with the green box in Fig. 7 and corresponds to the spark ignition stage in Fig. 5. After that, the kernel continues growing from $t = 1.5$ ms to $t = 2.0$ ms, which reflects the stage $t_1 - t_2$ in Fig. 5. The flame continuously grows inside the recirculation zone during 2.5 - 6.0 ms (within the brown box in Fig. 7). Then, the flame spreads rapidly until the fully burning combustion in the chamber is reached at t_3 .

Fig. 8 shows the evolution of the flame characteristic quantities (including flame projection area ΔS , length L , and width W) during a spark ignition process. Their extraction method is introduced in Section 2.4. Note that the milestone instants marked in Fig. 8, i.e., t_0 - t_3 , correspond to those in Fig. 5. At $t = t_0$, the flame is not discernible due to intense exposure to the spark discharge. An unstable flame kernel located inside the flameholder is created by electro-discharge from t_0 to t_1 . The corresponding flame projection area, length, and width are high at t_0 but decrease rapidly within t_0 - t_1 . Then they start to increase at t_1 . The kernel is generated and evolves from t_1 to t_2 . The above characterizes the initial ignition process, during which the flame kernel generates in the recirculation zone since the spark plug discharges. Afterward, the foregoing flame characteristic quantities rapidly increase to a constant value with considerable fluctuations, which indicates that stable combustion has been achieved. Moreover, the instant t_3 is deemed the beginning of continuous and stable combustion. Consequently, the flame projection area reaches its maximum value for the first time, marked as successful ignition. In our study, the instant t_3 is defined as the ignition delay time for the studied kerosene spray flames. The flame projection area fluctuations, length, and width during the flame development stage may be caused by the strong turbulence behind the flameholder.

3.2. Ignition delay time

The ignition delay time of spray kerosene flame in high-speed and low-pressure flows has not been mainly investigated, to the best of our knowledge. In this study, a number of experiments are conducted under various inlet pressure, Mach number, and temperature to measure the ignition delay time. All the measurements are performed at the global equivalence ratio of $\varphi_{total} = 0.082 \pm 0.004$. Fig. 9 shows the effects of the inlet pressure, Mach number, and temperature on the ignition delay time. The results are processed from at least three repeated experiments under the same condition. Generally, the results confirm the excellent repeatability of the tests and the accuracy of the image processing method. The uncertainties of length L and width W were 1.7% and 2.3%, respectively. Hence, the uncertainty of the ignition delay time was 2.89%. The exact instants, such as t_1 , are difficult, if not impossible, to be obtained without the specific features. In general, the spark ignition time t_1 is about 1.2 - 4.3 ms with the inlet temperature from 320 K to 800 K, which has little effect on ignition delay time, so this paper will not discuss this data in detail. The instants t_2 and t_3 share a similar tendency with a gap of 3.7 - 25.3 ms, which indicates that the spray flame evolves to a stable state from the generated kernel with an average duration of 9.4 ms.

Fig. 9(a) shows the time instants as functions of the inlet pressure when $Ma = 0.2$ and $T = 700$ K. It is seen that increase of the inlet pressure from 0.04 MPa to 0.08 MPa leads to a reduction of the ignition delay time t_3 (the black line) from 14.6 ms to 8.7 ms. It should be noted that an unexpected point is seen at $P_i = 0.06$ MPa, at which the ignition delay time t_3 is 5.8 ms. This unusual phenomenon may be caused by the difference in flame evolution. The flame projection area in a stable combustion state increases gradually with inlet pressure. It is widely accepted that the increase in pressure is beneficial to combustion; however, the ignition delay time is evaluated by the flame projection area in this work. The flame morphology obtained by the high-speed cam-

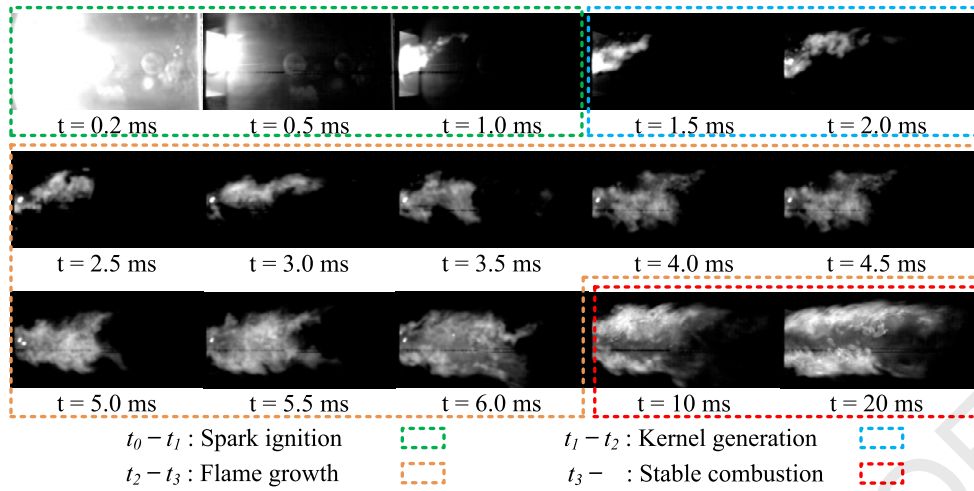


Fig. 7. Spray flame ignition process under $P_i = 0.06$ MPa, $Ma = 0.2$, $T = 700$ K and $\varphi_{total} = 0.082$. (For interpretation of the colors in the figures, the reader is referred to the web version of this article.)

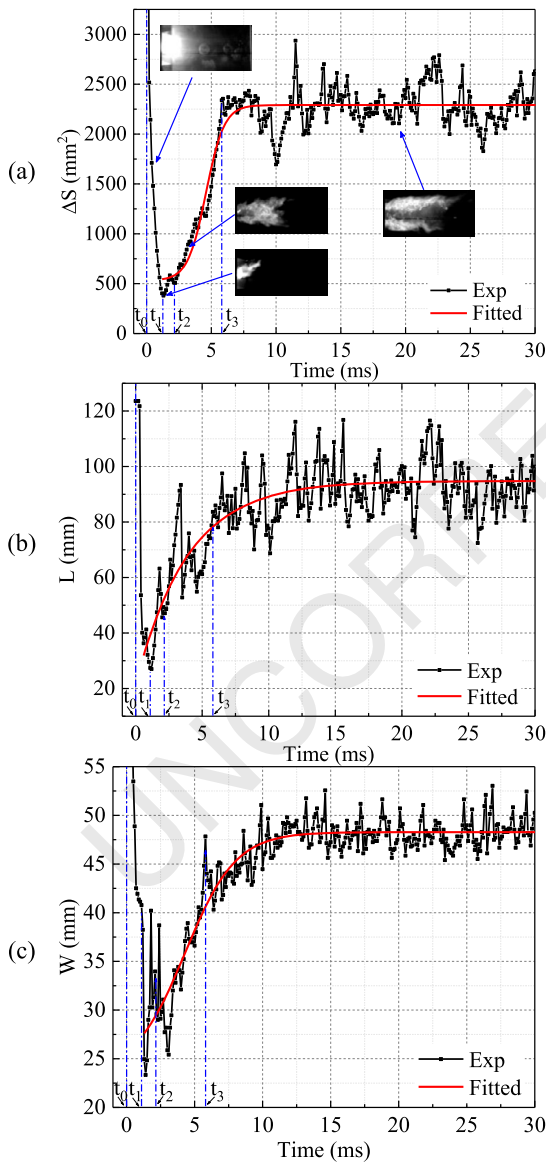


Fig. 8. Evolution of (a) flame projection area, (b) length, and (c) width during the ignition process. $P_i = 0.06$ MPa, $Ma = 0.2$, $T = 700$ K, $\varphi_{total} = 0.082$.

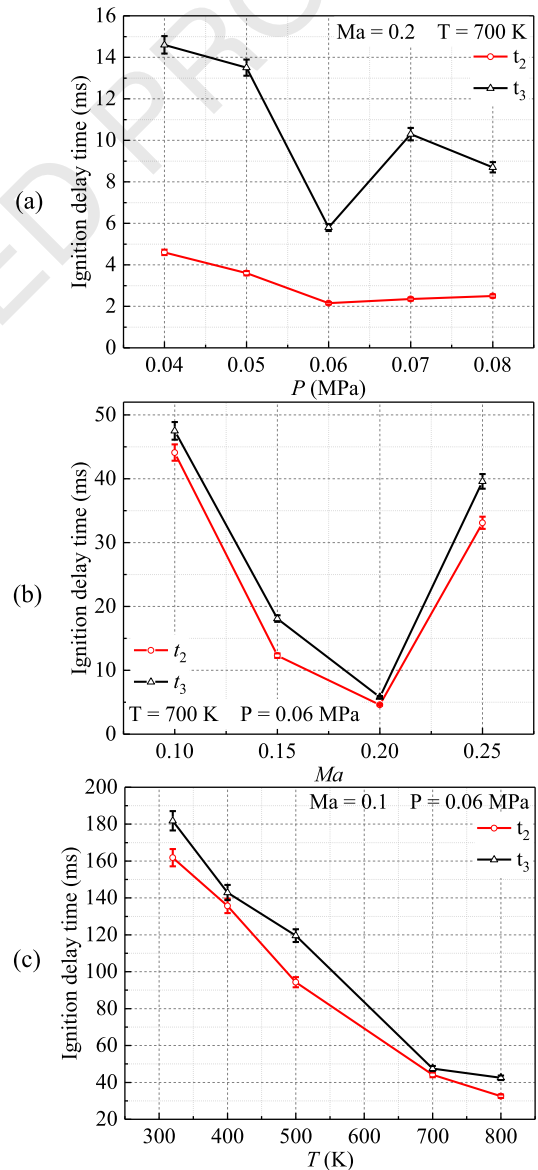


Fig. 9. Ignition delay time with different inlet conditions: (a) pressure, (b) Mach number, and (c) temperature.

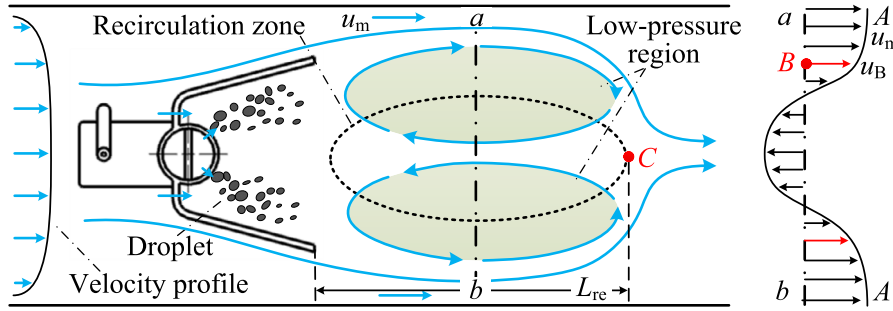


Fig. 10. Schematic of flame stability principle in the recirculation zone.

era shows that the maximum flame projection areas at $P_i = 0.07$ MPa and $P_i = 0.08$ MPa are 35.7% and 69.0% larger than that at $P_i = 0.06$ MPa, which increases the time for the flame projection area to reach its maximum. Therefore, the ignition delay time t_3 corresponding to the inlet pressure of 0.06 MPa is relatively small. Besides, a similar trend is achieved for t_2 , which reflects the acceleration of the chemical reaction rate by increased inlet pressure. At the same time, the stronger aerodynamic force can be obtained by higher density because of higher pressure, which facilitates the shattering of the fuel droplets. Meanwhile, at higher pressure, higher density leads to a larger air mass flow rate, which results in increased fuel mass flow rate at the constant equivalence ratio and Mach number. Hence, the droplet's initial size decreases rapidly because the squared pressure drop of the nozzle increases in proportion to the fuel mass flow rate. It is well known that smaller droplet size is beneficial for fuel evaporation and combustion, reducing the ignition delay time.

Fig. 9(b) shows the counterpart results when the inlet Mach number varies from 0.1 to 0.25. One can see that the instants t_2 and t_3 decrease first and reach their minimum values at $Ma = 0.2$. Then they increase as the inlet Mach number varies from 0.2 to 0.25. The shortest t_3 (5.8 ms) is obtained at $Ma = 0.2$, which is 87.79% lower than that at $Ma = 0.1$. The inlet Mach number has competitive effects on flame stabilization. On the one hand, increased Mach number can enhance flame stability by reducing the droplet diameter with a stronger aerodynamic force. On the other hand, higher speed means shorter residence time of fuel/air mixture in the combustor, which is expected to weaken the flame stability. Therefore, the ignition delay time presents a V-shaped trend with inlet Mach number, and an optimal Mach number exists to achieve the shortest ignition delay time. Here, the optimal Mach number (Ma_0) is about 0.2.

Fig. 9(c) shows air inlet temperature influences the instants of t_2 and t_3 . The Mach number is fixed to be 0.1, while the inlet pressure is 0.06 MPa. It is found that the ignition delay time t_3 decreases as the inlet temperature increases from 320 K to 800 K. Specifically, the ignition delay time reduces significantly from 181.8 ms to 47.5 ms with the temperature increases from 320 K to 700 K. After that, when the temperature increases to 800 K, the ignition delay time is reduced by only 10.5%. As mentioned above, the temperature increase reduces the ignition delay time by enhancing liquid fuel evaporation and improving the chemical reaction rate.

3.3. Flame stability limit

Flame stability limits are often used to describe the engine operation range, within which it can work safely without any global extinction propensity [28]. The critical parameters related to the operation range include inlet pressure, Mach number, and temperature. In this study, the equivalence ratio corresponding to the lowest fuel pressure drop, in which the fuel/air mixture can be critically ignited, is regarded as the lean ignition equivalence ra-

tio [29]. Besides, the lean blowout equivalence ratio corresponds to the lowest fuel/air ratio, with which the visible flame gradually shrinks to global extinction due to decreased fuel mass flow rate and would not be reignited when further increasing the fuel supply. Here, φ_{total} represents the total equivalence ratio calculated by the fuel mass flow rate and total air mass flow rate.

In our work, the spray flames under sub-atmospheric pressure conditions are stabilized by the recirculation zone downstream of the flameholder. Fig. 10 schematically demonstrates the mechanism of flame stability in our configurations. The fuel droplets are well mixed with the air in the evaporation tube, and the fuel/air mixture is formed along with the evaporation of droplets. After successful ignition, the flame is stabilized in the recirculation zone. Then, the flame propagation speed u_f that satisfies $0 < u_f < u_m$. Thus, in section a-b with the velocity profile A-A, a point B, whose velocity u_B is equal in magnitude and opposite in direction to the u_f , is $u_B = u_f$. However, the stable flame in section a-b is only a schematic diagram, where the position of the section a-b may be upstream or downstream in the recirculation zone. Generally, the ignited flame always happens in the downstream area, and then the burned gas moves upstream along the reflux to ignite the fresh fuel/air mixture, forming a stable flame. Hence, critical point C, namely the furthest downstream point where the flame can be ignited and stabilized, is located at the end of the recirculation zone.

According to the analytical stationary state described above, if the energy carried by the recirculating burned gas can ignite the fresh fuel/air mixture, the flame is considered to be stable; otherwise, extinction will occur. However, the dual-vortex, which formed the circulation zone, sheds downstream alternately with the high frequency. Therefore, it is difficult to analyze the principle of flame stability from the perspective of reflux energy, and there is no theoretical basis. Thus, the flame stability principle in the recirculation zone can be well understood by the characteristic time scale theory [30], which indicates that a stable flame is achieved if the mixture residence time, τ_{flow} is longer than the ignition delay time, τ_i [31,32]. The ignition delay time is usually determined as the Arrhenius form [18]:

$$t_i = A[P]^\alpha [\varphi]^\gamma [X_{O_2}]^\delta \exp(E/RT) \quad (5)$$

where the A is a constant, P is the inlet pressure, φ is the equivalence ratio of the evaporated gas fuel, X_{O_2} is the volume fraction of O_2 , E is the activation energy, R is the universal gas constant, T is the inlet temperature, $\gamma > 0$ is the constant, α and δ are the influence factors. Here, the $[X_{O_2}]^\delta$ is the constant with the constant volume fraction of O_2 .

The mixture residence time, τ_{flow} is defined as the period during the fuel/air mixture entering into the recirculation zone to leaving, that is

$$\tau_{flow} = \frac{L_{re}}{u_m} \quad (6)$$

where L_{re} is the characteristic length of the recirculation zone downstream of the flameholder, u_m is the mainstream velocity. Here, the L_{re} is proportional to the width of the stabilizer, which can be considered as a constant, and $u_m = Ma(kRT)^{1/2}/(1 - \beta)$. Thus,

$$\tau_{flow} = \frac{L_{re}(1 - \beta)}{Ma\sqrt{kRT}} \propto Ma^{-1}T^{-0.5} \quad (7)$$

Given that the lowest equivalence ratio φ of the evaporated gas fuel, which leads to the critical state, expressed as $\tau_{flow} = \tau_i$, then

$$[P]^\alpha [\varphi]^\gamma \exp(E/RT) \propto Ma^{-1}T^{-0.5} \quad (8)$$

and

$$\varphi \propto \varphi_{total}\lambda_r \quad (9)$$

where the λ_r is the effective evaporation, mostly affected by temperature and initial particle size.

Therefore, Eq. (8) can be simplified by Eq. (1), Eq. (9), and Eq. (10), yielding

$$\varphi_{total} \propto Ma^\alpha P^\delta \left[\frac{1}{T} \exp\left(-\frac{E}{RT}\right) \right]^\varepsilon \left(\frac{1}{\lambda_r}\right)^\gamma \quad (10)$$

where the α , δ , ε , and γ are the influence factors.

Assume that

$$\theta(T) = \frac{1}{T} \exp\left(-\frac{E}{RT}\right) \quad (11)$$

$$\zeta(T) = \frac{1}{\lambda_r} \quad (12)$$

we have

$$\varphi_{total} \propto Ma^\alpha P^\delta \theta(T)^\varepsilon \zeta(T)^\gamma \quad (13)$$

It is seen that the $\zeta(T)$, reflecting the evaporation of the fuel droplets, decreases with the temperature increases, and the initial particle size reduces. Besides, the $\theta(T)$ decreases when T varies from 320 K to 800 K. The above analysis indicates that the equivalence ratios of lean ignition and blowout are affected by inlet pressure, Mach number, and temperature. Below the quantitative analysis will be made based on the experimental measurements.

3.3.1. Effects of inlet pressure

Plotted in Fig. 11 are the flame stability limits as functions of different inlet pressures. Three Mach numbers are considered, whilst the inlet temperature is fixed to be $T = 700$ K. In general, the stable flame regime is extended as the inlet pressure increases. Linear variations are obtained at $Ma = 0.1$, as shown in Fig. 11(a), where the ignition equivalence ratios φ_{IG} decrease from 0.111 to 0.012 with the pressure increases from 0.05 MPa to 0.1 MPa. Moreover, the extinction limits are slightly lower than the ignition limits, and the mean equivalence ratio of a lean blowout is 9.93% smaller than that of ignition. The non-linear (faster decreasing) tendencies can be observed with $Ma = 0.15$ and 0.2. In Fig. 11(b), the inlet Mach number is 0.15, the lowest pressure that can be ignited successfully is 0.03, where the equivalence ratios of ignition φ_{IG} and lean blowout φ_{LBO} are 0.168 and 0.147, respectively. As the inlet pressure increases from 0.03 MPa to 0.10 MPa, the ignition equivalence ratio first decreases rapidly to 0.060 at $P_i = 0.06$ MPa and then slowly to 0.014 at $P_i = 0.10$ MPa.

As can be seen in Fig. 11(c), the ignition equivalence ratio φ_{IG} decreases from 0.105 to 0.015 as the inlet pressure increases from 0.04 MPa to 0.10 MPa. Meanwhile, the lowest lean blowout equivalence ratio φ_{LBO} obtained at 0.10 MPa is 0.01, which is 87.93% smaller than that at 0.04 MPa. All of the lean blowout φ_{LBO} are

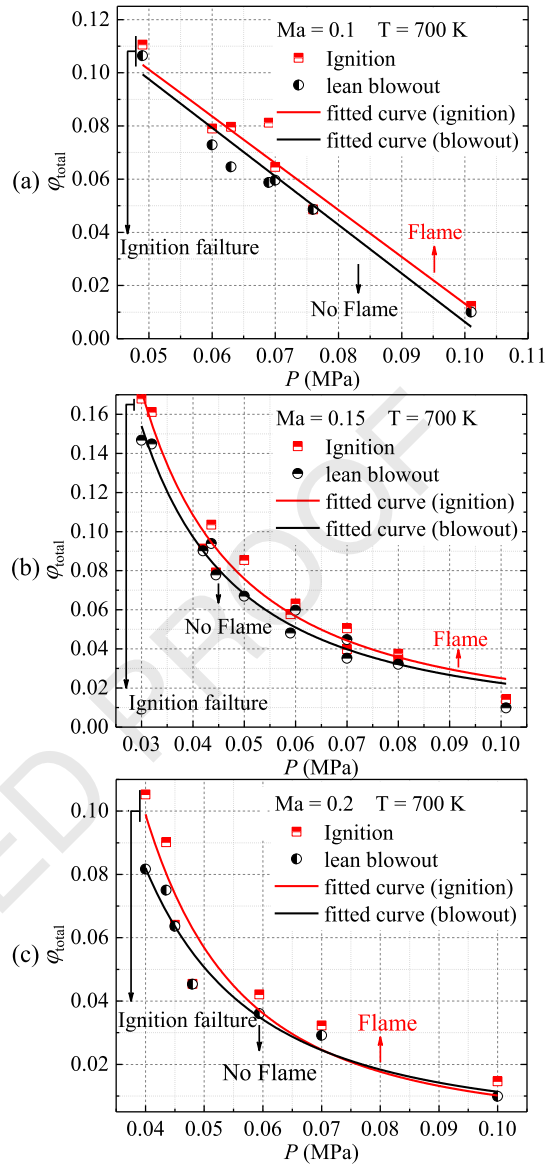


Fig. 11. Ignition and blowout limits with different inlet pressures: (a) $Ma = 0.1$, (b) $Ma = 0.15$, (c) $Ma = 0.2$. The inlet temperature is $T = 700$ K.

close to the equivalence ratio of ignition φ_{IG} , whose averaged values at $Ma = 0.1$, 0.15, and 0.2 are 9.83%, 12.01%, and 15.65% larger than that of the lean blowout, respectively. Besides, the difference between the equivalence ratios of ignition φ_{IG} and lean blowout φ_{LBO} decreases with inlet pressure. This implies that the flameholder in Fig. 2 has excellent flame stability even in ultra-low pressure. However, a reduction in inlet pressure would eventually cause ignition failure. The minimum pressure required to stabilize the flame is 0.049, 0.03, and 0.04 MPa, respectively, corresponding to the Mach number of $Ma = 0.1$, 0.15, and 0.2.

When the inlet Mach number and temperature are constant, the $\theta(T)$ is constant, and the variation of $\zeta(T)$ is slight. Then, the equivalence ratios of lean ignition and blowout depend on the pressure following $\varphi \propto P^\delta$. The exponents depend on the flameholder configuration in the sub-atmospheric environment. At $Ma = 0.1$, the equivalence ratios of lean ignition φ_{IG} and blowout φ_{LBO} are linear with the pressure (see Fig. 11a), and therefore $\delta = 1$. When the Mach numbers are 0.15 and 0.2, the flame stability limits decrease exponentially with the inlet pressure. The exponents δ are evaluated as about -1.6 and -2.5 , respectively corresponding

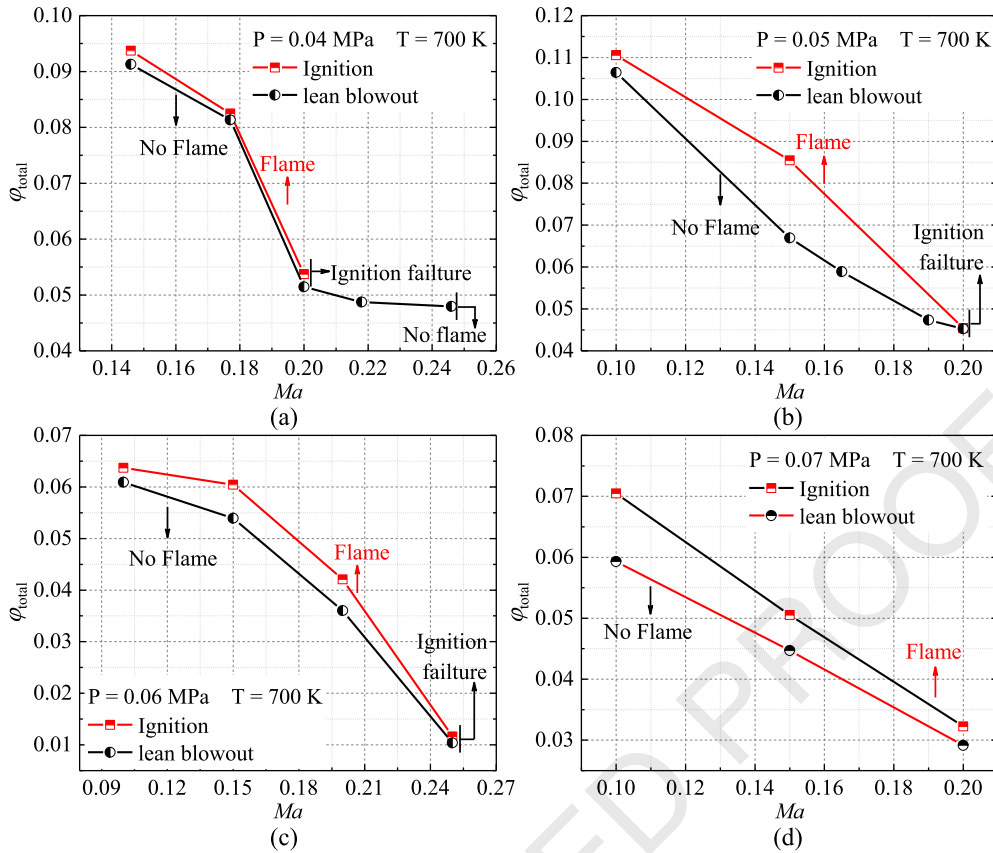


Fig. 12. Ignition and blowout limits with different inlet Mach number with (a) 0.04 MPa; (b) 0.05 MPa; (c) 0.06 MPa; (d) 0.07 MPa. The inlet temperature is 700 K.

to $Ma = 0.15$ and 0.2 . For lean blowout, the pressure exponents δ are -1.596 and -2.160 for the preceding Mach numbers. This is because the stability of spray combustion is jointly affected by pressure and air velocity.

3.3.2. Effects of Mach number

Fig. 12 shows the influence of Mach number on the ignition and blowout limits at inlet temperature $T = 700$ K. Four pressures are considered, i.e., 0.04, 0.05, 0.06, and 0.07 MPa. As shown in Fig. 12(a), the ignition equivalence ratio φ_{IG} reduces quickly from 0.094 to 0.054 as the Mach number varies from 0.15 to 0.2, and the ignition failure occurs when the Mach number is larger than 0.2. However, if the Mach number continues to increase after successful ignition is achieved, it is found that the flame would still be stable in the Mach number range of 0.2 – 0.246. When the inlet pressure is 0.06 MPa in Fig. 12(c), as the Mach number increases from 0.1 to 0.15, the ignition equivalence ratio φ_{IG} slowly decreases from 0.064 to 0.060. When the Mach number increases from 0.15 to 0.25, the ignition equivalence ratio φ_{IG} rapidly drops to 0.012. The same tendency is also observed for the lean blowout limit and the lean blowout equivalence ratio φ_{LBO} reduces from 0.061 to 0.010, when the Mach number increases from 0.1 to 0.25. Besides, the equivalence ratio boundary between successful ignition and extinction gradually narrows with increasing inlet velocity. Note that the flame cannot be stabilized when $Ma > 0.25$.

Increased Mach number would lead to two opposite effects. First, the acceleration of the air stream shortens the mixture residence time. It may also increase the aerodynamic force and hence enhance the shattering of fuel droplets. However, increased Mach number reduces φ_{IG} and φ_{LBO} when the Mach number is large enough, the flame still cannot be stable, and there exists a limiting Mach number. Furthermore, when the inlet pressure and temper-

ature are constant, Eq. (13) shows that the flame stability limit is positively related to the Mach number, which is expressed as $\varphi_{total} \propto Ma^\alpha \zeta(T)^\gamma$. Assume that at the same equivalent ratio, increased Mach number would increase the airflow rate \dot{m}_{air} . Therefore, according to $q = \dot{m}_{fuel}/\dot{m}_{air}$ and $\varphi = q/q_{st}$, the fuel mass flow rate \dot{m}_{fuel} also increases with an increase in fuel pressure drop ΔP . Then the diameter of initial fuel droplets decreases, leading to a decrease in $\zeta(T)$, which improves the flame stability. Hence, the equivalence ratio of flame stability limit decreases. An interesting phenomenon is that a more substantial point extinction gap is obtained near the Mach number 0.14. This indicates that the extinction limits can be extended effectively with the optimum Mach number range under an individual evaporation rate at $T = 700$ K, and it may change with the inlet temperature.

3.3.3. Effects of inlet temperature

The effects of inlet temperature on flame stability limits are presented in Fig. 13. The equivalence ratio of lean ignition φ_{IG} and blowout φ_{LBO} changes differently with the inlet temperature. Specifically, the ignition equivalence ratio φ_{IG} decreases first and then increases as the inlet temperature increases. The temperature corresponding to the inflection point rises from 400 K to 700 K as the Mach number gradually increases from 0.1 to 0.2. At $Ma = 0.1$ and $P_i = 0.06$ MPa, the blowout equivalence ratio φ_{LBO} increases approximately linearly from 0.032 to 0.050 when the inlet temperature increases from 320 K to 800 K. The minimum temperature of successful ignition is 320 K at $Ma = 0.1$, and it becomes 510 K at $Ma = 0.2$. Additionally, the equivalence ratio of a lean blowout φ_{LBO} is 12.87% smaller than ignition, and the gap narrows as the temperature rises. Again, this phenomenon shows that the fuel evaporates in the evaporation tube helps improve flame stability.

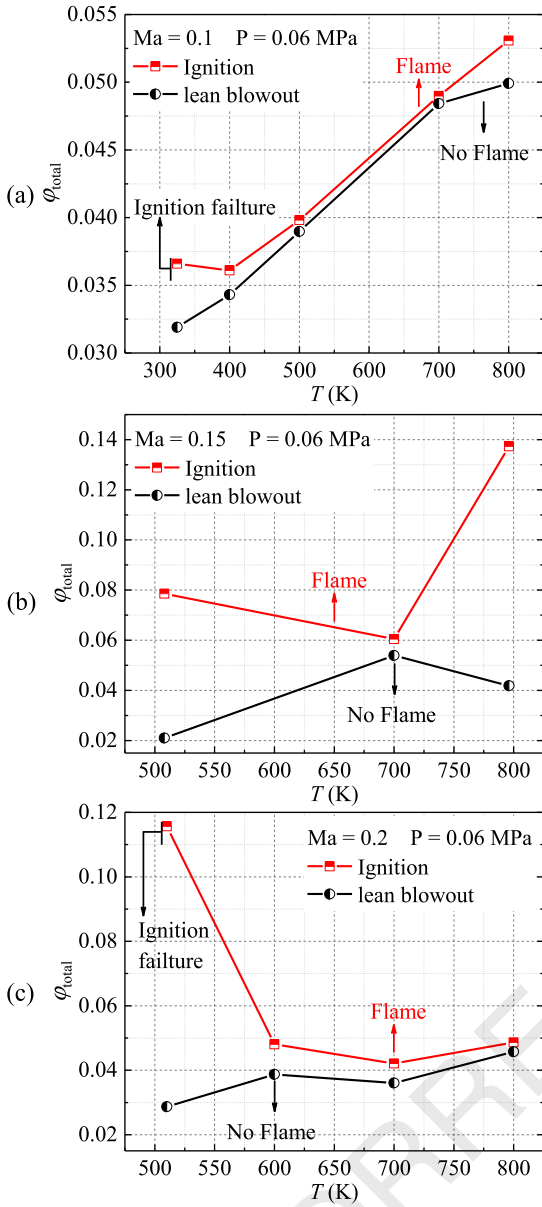


Fig. 13. Ignition and lean blowout limits with different inlet temperatures with (a) $Ma = 0.1$; (b) $Ma = 0.15$; (c) $Ma = 0.2$. The inlet pressure is 0.06 MPa.

Typically, better evaporation of fuel and a higher chemical reaction rate can be achieved by the increased inlet temperature. The equivalence ratios of ignition and extinction decrease with temperature, but our measurements show the opposite results. It is mainly because, with a constant Mach number, increased inlet temperature may increase the absolute velocity, which would weaken flame stabilization. As analyzed previously, poor atomization can occur with a lower fuel mass flow rate, reducing the flame stabilization boundary. When the inlet pressure and Mach number remain constant, Eq. (10) can be given as

$$\varphi_{total} \propto \theta(T)^\varepsilon \zeta(T)^\gamma \quad (14)$$

Here $\theta(T)$ and $\zeta(T)$ decrease with temperature, indicating that the fuel evaporation and chemical reaction rate can be enhanced, and the equivalence ratio φ_{total} thus decreases. However, the reduction of \dot{m}_{fuel} reduces the fuel droplets diameter and $\zeta(T)$. Therefore, flame stability is influenced by these two aspects. Under low inlet temperature conditions, slightly increased tempera-

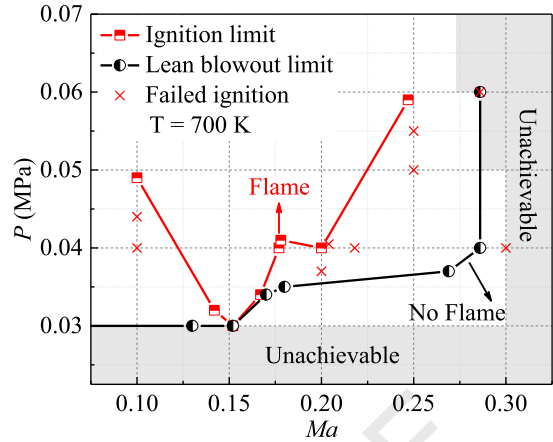


Fig. 14. Envelope of stable spray kerosene combustion under sub-atmospheric conditions. Inlet temperature: $T = 700$ K.

ture can significantly improve fuel evaporation and chemical reaction rate, which makes the ignition equivalence ratio φ_{IG} drop. Whereas, with temperature increases to a certain extent, the fuel evaporation and chemical reaction rate will not change much, but the absolute inlet velocity will increase, leading to an increase in the ignition equivalence ratio. Besides, lean blowout measurements are carried out after ignition. The evaporation tube has already been preheated, and the evaporation effect is mainly related to the gas temperature inside the chamber. Therefore, instead of increasing the evaporation rate, raising the temperature would increase the gas velocity, thus increasing the lean blowout equivalence φ_{LBO} .

3.3.4. Stability envelope

The biggest challenge of ignition or reignition is the extreme conditions at the high-speed and high altitude. The combustor's inlet pressure and temperature are the ultra-low and worth focus. Conventionally, the envelope of stable combustion in a combustor can be parameterized with critical parameters, e.g., inlet pressure, Mach number, and temperature. The parametric boundary (inlet pressure versus inlet Mach number) for stable spray kerosene flames is illustrated in Fig. 14. The red curve is the lowest pressure or Mach number, which can ignite successfully, whereas the black one is the lowest condition with which a stable flame can exist. The red "x" indicates the failed ignition under the corresponding conditions. The shaded region shows the states which have not been measured. If the inlet temperature is constant, Eq. (11) can be written as $\varphi \propto Ma^\alpha P^\delta$, where δ is $-0.1596 - 0.2486$. This indicates that reduced lean ignition and blowout equivalence ratios are achieved by decreased Mach number or increased inlet pressure. Therefore, there must exist a limit of pressure or Mach number, with which the flameholder cannot stabilize the flame. Generally, the flame stability boundary is fixed and unique. The limitations of pressure or Mach number for ignition and lean blowout are almost not changed. However, due to the evaporation effect of the evaporation tube in the combustion state, the lean blowout limits are more comprehensive than the ignition limits. This conclusion is also confirmed by Fig. 12(a); when the inlet Mach number is larger than 0.2, the flame cannot be ignited by the spark plug, while the flame can still be stabilized. The test is achieved by ignited first and then changing the inlet Mach number larger than 0.2.

As can be seen in Fig. 14, the minimum pressure to stabilize the flame decreases first and then increases with the Mach number, and the lowest pressure is achieved at $Ma = 0.15$. Moreover, the Mach number increases with pressure. The lowest pressure of 0.03

MPa with which the ignition succeeds appears at $Ma = 0.15$. Usually, the lean blowout boundary is wider than the ignition boundary, mainly because the burning flame promotes fuel evaporation. At 0.059 MPa, the maximum Mach number for successful flame ignition is 0.247, and the flame can stabilize when the Mach number is less than 0.286. This indicates that successful reignition will happen after the combustion extinction occurs in the flight state after the aircraft coasts into the combustion conditions of higher pressure or lower Mach number.

4. Conclusions

The spray kerosene flame stability limits and ignition delay time are experimentally studied in the subatmospheric environment at the pressure of 0.03 – 0.06 MPa, Mach number of 0.1 – 0.3, and temperature of 320 K – 800 K. The flame stability limits are identified by the lean ignition and blowout equivalence ratios and the envelope of stable combustion. The ignition delay time is evaluated by flame morphology measured by a high-speed camera. The experimental results of ignition delay time and flame stability limit in the subatmospheric pressure environment are beneficial for exploring near space vehicles' design. The main conclusions are summarized as follows:

- (1) The equivalence ratios of lean ignition and blowout decrease for spray combustion with the increase of pressure. An increase in Mach number reduced the equivalence ratios of flame stability, but there exists a maximum Mach number of flame stabilization. The ignition equivalence ratio decreases first and then increases as the temperature increases, while the lean blowout equivalence ratio increases with temperature. The minimum temperature with which the ignition failure occurs rises when the Mach number varies from 0.1 to 0.2.
- (2) The empirical correlation between the equivalence ratios of flame stability and inlet parameters, such as pressure, Mach number, temperature, is developed and verified in this study.
- (3) Four stages are observed of the ignition process: enveloped flame core, kernel generation, flame growth, and stable combustion. The formation time of enveloped flame core decreases slightly with temperature, and it is independent of inlet pressure and Mach number (about 1.2 ms at 700 K). It is also found that kernel generation is crucial to the success of ignition.
- (4) The reduction of ignition delay time is achieved by increased pressure or temperature. The ignition delay time presents a concave-type shape with the increase of inlet Mach number.

Declaration of competing interest

The authors declare that they have no known competing financial interests or personal relationships that could have appeared to influence the work reported in this paper.

Acknowledgement

This work was supported by the National Science and Technology Major Project (No. 2017-III-0008-0034). YH gratefully acknowledges the financial support from the China Scholarship Council (No. 201906830096).

References

- [1] S. Chen, D. Zhao, Numerical study of non-reacting flowfields of a swirling trapped vortex ramjet combustor, *Aerosp. Sci. Technol.* 74 (2018) 81–92, <https://doi.org/10.1016/j.ast.2018.01.006>.
- [2] G. Choubey, Y. D. W. Huang, L. Yan, H. Babazadeh, K.M. Pandey, Hydrogen fuel in scramjet engines - a brief review, *Int. J. Hydrog. Energy* 45 (2020) 16799–16815, <https://doi.org/10.1016/j.ijhydene.2020.04.086>.

- [3] L. Shi, G. Zhao, Y. Yang, F. Qin, X. Wei, G. He, Experimental study on ejector-to-ramjet mode transition in a divergent kerosene-fueled RBCC combustor with low total temperature inflow, *Aerosp. Sci. Technol.* 99 (2020) 105734, <https://doi.org/10.1016/j.ast.2020.105734>.
- [4] W. Huang, L. Yan, J.G. Tan, Survey on the mode transition technique in combined cycle propulsion systems, *Aerosp. Sci. Technol.* 39 (2014) 685–691, <https://doi.org/10.1016/j.ast.2014.07.006>.
- [5] G. Choubey, Y. Devarajan, W. Huang, K. Mehar, M. Tiwari, K.M. Pandey, Recent advances in cavity-based scramjet engine - a brief review, *Int. J. Hydrog. Energy* 44 (2019) 13895–13909, <https://doi.org/10.1016/j.ijhydene.2019.04.003>.
- [6] D. Szirczak, H. Smith, A review of design issues specific to hypersonic flight vehicles, *Prog. Aerosp. Sci.* 84 (2016) 1–28, <https://doi.org/10.1016/j.paerosci.2016.04.001>.
- [7] M. Colket, T. Edwards, W.M. Roquemore, W. International, W. Lake, D. Turner, R. Royce, N. American, Overview of the national jet fuels combustion program 55 (2017), <https://doi.org/10.2514/1.J055361>.
- [8] Z.G. Niu, L.Q. Fei, S.Y. Feng, X.M. He, Experiment on combustion performance of a ramjet prototype combustor in low pressure condition, *J. Propuls. Technol.* (32) (2011) 509–511, <https://doi.org/10.1080/17415993.2010.547197>.
- [9] K. Okai, T. Himeno, T. Watanabe, H. Kobayashi, H. Taguchi, Investigation of combustion and altitude-ignition performance of a small hydrogen-fueled reversed-flow turbine combustor, in: 52nd Aerosp. Sci. Meet., 2014, pp. 1–9.
- [10] Z. Wu, X. Zhou, X. Liu, Y. Ni, K. Zhao, F. Peng, L. Yang, Investigation on the dependence of flash point of diesel on the reduced pressure at high altitudes, *Fuel* 181 (2016) 836–842, <https://doi.org/10.1016/j.fuel.2016.05.062>.
- [11] Y. Fu, S. Lu, L. Shi, X. Cheng, H. Zhang, Ignition and combustion characteristics of lithium ion batteries under low atmospheric pressure, *Energy* 161 (2018) 38–45, <https://doi.org/10.1016/j.energy.2018.06.129>.
- [12] D.O. Black, W.E. Messing, Effect of three flame-holder configurations on subsonic flight performance of rectangular ram jet over range of altitudes, *NACA*, 1948.
- [13] J.S. Drabble, Investigation into the Performance of a "REID" Forced Air Blast Ramjet Combustion Chamber on a Low Pressure Combustion Rig, *NASA TN GW*, 1953.
- [14] W. Zeng, H.X. Li, B.D. Chen, H.A. Ma, Experimental and kinetic modeling study of ignition characteristics of Chinese RP-3 kerosene, *Combust. Sci. Technol.* 187 (2015) 396–409, <https://doi.org/10.1080/00102202.2014.948620>.
- [15] S. Yang, C. Zhang, Y. Lin, X. Xue, X. Gan, Experimental investigation of the ignition process in a separated dual-swirl spray flame, *Combust. Flame* 219 (2020) 161–177, <https://doi.org/10.1016/j.combustflame.2020.05.010>.
- [16] R.W. Read, J.W. Rogerson, S. Hochgreb, Relight imaging at low temperature, low pressure conditions, in: 46th AIAA Aerosp. Sci. Meet. Exhib., 2008.
- [17] D.N. Nguyen, H. Ishida, M. Shioji, Ignition and combustion characteristics of gas-to-liquid fuels for different ambient pressures, *Energy Fuels* 24 (2010) 365–374, <https://doi.org/10.1021/ef9008532>.
- [18] B.H. Chen, J.Z. Liu, F. Yao, Y. He, W.J. Yang, Ignition delay characteristics of RP-3 under ultra-low pressure (0.01–0.1 MPa), *Combust. Flame* 210 (2019) 126–133, <https://doi.org/10.1016/j.combustflame.2019.08.009>.
- [19] Y. Zhang, X. He, H. Zhu, Study on atomization performance of multi-orifice air-assisted plain jet atomizers, *Fuel* 286 (2021) 119428, <https://doi.org/10.1016/j.fuel.2020.119428>.
- [20] F. Chen, C. Ruan, T. Yu, W. Cai, Y. Mao, X. Lu, Effects of fuel variation and inlet air temperature on combustion stability in a gas turbine model combustor, *Aerosp. Sci. Technol.* 92 (2019) 126–138, <https://doi.org/10.1016/j.ast.2019.05.052>.
- [21] P. Jiang, X. He, Experimental investigation of flow field characteristics in a mixed-flow trapped vortex combustor, *Aerosp. Sci. Technol.* 96 (2020) 105533, <https://doi.org/10.1016/j.ast.2019.105533>.
- [22] L. Wermer, ur na l P re of, *Colloids Surf. A, Physicochem. Eng. Asp.* (2020) 124658, <https://doi.org/10.1016/j.energy.2020.119162>.
- [23] P. Jiang, X. He, Performance of a novel mixed-flow trapped vortex combustor for turboshaft engine, *Aerosp. Sci. Technol.* 105 (2020) 106034, <https://doi.org/10.1016/j.ast.2020.106034>.
- [24] J. Liu, E. Hu, W. Zeng, W. Zheng, A new surrogate fuel for emulating the physical and chemical properties of RP-3 kerosene, *Fuel* 259 (2020) 116210, <https://doi.org/10.1016/j.fuel.2019.116210>.
- [25] J. Fan, D.K.Y. Yau, A.K. Elmagarmid, W.G. Aref, Automatic image segmentation by integrating color-edge extraction and seeded region growing, *IEEE Trans. Image Process.* 10 (2001) 1454–1466, <https://doi.org/10.1109/83.951532>.
- [26] F. Xing, A. Kumar, Y. Huang, S. Chan, C. Ruan, S. Gu, X. Fan, Flameless combustion with liquid fuel: a review focusing on fundamentals and gas turbine application, *Appl. Energy* 193 (2017) 28–51, <https://doi.org/10.1016/j.apenergy.2017.02.010>.
- [27] S. Zhao, Y. Fan, Experimental and numerical study on thermodynamic performance in a designate pilot-ignition structure: step, *Aerosp. Sci. Technol.* 91 (2019) 561–570, <https://doi.org/10.1016/j.ast.2019.05.049>.
- [28] F. Williams, *Combustion Theory*, second ed., Addison-Wesley, Reading, MA, 1985.

- 1 [29] A.H. Lefebvre, D.R. Ballal, Gas Turbine Combustion, third ed., Taylor & Francis
2 Group, New York, 2010. 67
- 3 [30] S.G. Tuttle, S. Chaudhuri, S. Kostka, K.M. Kopp-Vaughan, T.R. Jensen, B.M. Cete- 68
4 gen, M.W. Renfro, Time-resolved blowoff transition measurements for two- 69
5 dimensional bluff body-stabilized flames in vitiated flow, Combust. Flame 159 70
6 (2012) 291–305, <https://doi.org/10.1016/j.combustflame.2011.06.001>. 71
- 7 72
8 73
9 74
10 75
11 76
12 77
13 78
14 79
15 80
16 81
17 82
18 83
19 84
20 85
21 86
22 87
23 88
24 89
25 90
26 91
27 92
28 93
29 94
30 95
31 96
32 97
33 98
34 99
35 100
36 101
37 102
38 103
39 104
40 105
41 106
42 107
43 108
44 109
45 110
46 111
47 112
48 113
49 114
50 115
51 116
52 117
53 118
54 119
55 120
56 121
57 122
58 123
59 124
60 125
61 126
62 127
63 128
64 129
65 130
66 131
132
- [31] X. Cheng, Y. Fan, Experimental study of lean ignition and lean blowout perfor-
mance improvement using an evaporation flameholder, Int. J. Heat Mass Transf.
103 (2016) 319–326, <https://doi.org/10.1016/j.ijheatmasstransfer.2016.07.003>.
- [32] T.Y. Kim, Y.H. Kim, Y.J. Ahn, S. Choi, O.C. Kwon, Combustion stability of in-
verse oxygen/hydrogen coaxial jet flames at high pressure, Energy 180 (2019)
121–132, <https://doi.org/10.1016/j.energy.2019.05.089>.

UNCORRECTED PROOF